Error estimation and adaptivity

Stéphane Bordas

Marc Duflot

EPSRC summer school: University of Glasgow

August 26 – September 1, 2007

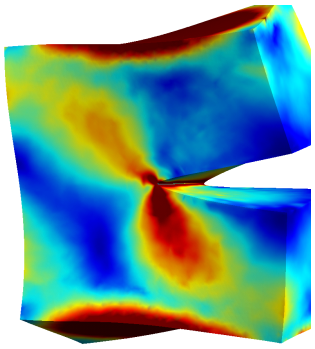

This page intentionally contains only this sentence.

Contents

This page intentionally contains only this sentence.

List of Figures

Chapter 1

Different kinds of errors in numerical methods

"While verification and validation and uncertainty quantification have been subjects of concern for many years, their further development will have a profound impact on the reliability and utility of simulation methods in the future. [...] As they stand now, verification, validation, and uncertainty quantification are challenging and necessary research areas that must be actively pursued." — National Science Foundation (USA) — Simulation-Based Engineering Science, final report

1.1 Why do we need error estimates?

Simulation-based engineering is concerned with solving physical problems of interest to engineers with a computer. Several questions must be answered for this: (i) How can the physical problem be modelled, i.e. what are the equations describing the phenomenon? This leads to a mathematical model. (ii) How can these equations be re-worked into a computational model (finite element, boundary element, meshfree, etc.) to be solvable on a computer? Assuming these two questions were suitably answered and a numerical solution obtained, one might wonder (iii) *"Are the equations solved correctly and what is the error?"*

The importance of error estimation when solving physical problems numerically (discretely) is clear. The first source of error lies in the construction of the mathematical model, the second, is related to the error committed by the numerical model (discretised version of the mathematical model). Szabó and Babuška suggest that knowledge of the error is essential to be able to correlate experimental and numerical results: one must ensure that the numerical results are close to the true solution of the mathematical model, to guarantee that any discrepancy between the numerical and experimental results can be ascribed to the unsuitability of the mathematical model. Strouboulis stated clearly the need for accurate error estimates for extended finite element methods [27].

Numerical methods, the finite element method (FEM) especially, revolutionalised industrial product development throughout engineering disciplines. The first error estimation paper dates back to Richardson in 1910 [22], in the context of finite differences. Shortly after the start of the FEM era, it became evident that validating and verifying the numerical schemes was vital for computer simulation to play any significant role in engineering analysis. The developments that followed led to a better understanding of what causes error, how this error is distributed and how the numerical method or the approximation can be modified to minimize this error: some key contributions in this respect are [2–4, 17, 19, 21, 30–32].

Figure 1.1: Sources of error in simulation.

U **Physical object/process**

$\Downarrow$

$\varepsilon_1 \longrightarrow$ **Error of the physical theory**

$\Downarrow$

u **Mathematical model** $Au = f$

$\Downarrow$

$\varepsilon_2 \longrightarrow$ **Approximation error**

$\Downarrow$

u_h **Discrete model** $A^h u_h = f_h$

$\Downarrow$

$\varepsilon_3 \longrightarrow$ **Computational error**

$\Downarrow$

u_h^ε **Numerical solution** $A^h u_h^\varepsilon = f_h + \varepsilon$.

1.2 When the standard FEM works and when it does not

In this part of the course, we will study the convergence of the finite element method. At the end of this section, you should be able to assess what the convergence rate of the FEM depends on, how it can be improved, and for which problems the FEM is not an appropriate method.

Let us write the physical problem in the following abstract form:

Find $u \in \mathcal{V}$, such that for all $v \in \mathcal{V}^0$ [1]

$$a(u,v) = (v,f) + (v,h)_\Gamma \tag{1.1}$$

where $a(\cdot,\cdot)$, $(\cdot,\cdot)$ and $(\cdot,\cdot)_\Gamma$ are symmetric bilinear forms [2].

For simplicity, but without loss of generality, we will now assume the of the first term in the right hand side of (1.2) –this corresponds to a linear elasticity problem without body forces– and we will note $(v,h)_\Gamma = F(v)$, where F is a linear form (since $(\cdot,\cdot)$ is bilinear).

Let us now define the approximate finite element problem:

Find $u_h \in \mathcal{V}_h$, such that for all $v_h \in \mathcal{V}_h^0$ [3]

$$a(u_h, v_h) = \underbrace{(v_h, f)}_{\text{0 since no body force}} + \underbrace{(v_h, h)_\Gamma}_{F(v_h)} = F(v_h) \tag{1.2}$$

Define the error due to the finite element approximation $e = u - u_h$, the following theorem holds:

Theorem 1.2.1. *Galerkin orthogonality*

For all functions v_h of $\mathcal{V}_h^0$, $a(v_h, e) = 0$, i.e. the error e is orthogonal to the space $\mathcal{V}_h$ in the sense of the bilinear form a. Or, equivalently, this means that u_h is the orthogonal (in the sense of a) projection of u on the subspace $\mathcal{V}_h$, as depicted in Figure 1.2.

[1] a function in $\mathcal{V}$ satisfies the essential boundary conditions, a function in $\mathcal{V}^0$ satisfies the corresponding homogeneous boundary conditions

[2] for the linear elasticity model problem in one space dimension, x: $a(u,v) = \int_\Omega u_{,x} v_{,x} d\Omega$, $(v,f) = \int_\Omega v f d\Omega$ and $(v,h) = \int_\Gamma v h d\Gamma$.

[3] we assume that the finite element spaces $\mathcal{V}_h$ and $\mathcal{V}_h^0$ are such that $\mathcal{V}_h \subset \mathcal{V}$ and $\mathcal{V}_h^0 \subset \mathcal{V}^0$

Theorem 1.2.2. *Best approximation property*

Any function U_h of $\mathcal{V}_h$ is a worse approximant (with respect to the energy norm associated with the bilinear form a) than the Galerkin finite element solution u_h. Mathematically, for all U_h of $\mathcal{V}_h$:

$$a(u_h - u, u_h - u) \underbrace{\equiv}_{\textit{definition}} a(e,e) \leq a(U_h - u, U_h - u) \tag{1.3}$$

This is known as the best approximation property of the Galerkin finite element method.

Remark. This best approximation property means that the finite element solution is a least-squares fit of the exact solution in the sence of the bilinear form a. This implies that the k^{th} first derivatives of u are fit best (in the sense of a) by the k^{th} derivative of finite element solution u_h. And, from a mechanics point of view, this means that the strains (stresses) are optimum.

Theorem 1.2.3. *Assume that the essential boundary conditions are homogeneous (i.e. $\mathcal{V}_h = \mathcal{V}_h^0$), then*

$$a(u,u) = a(u_h,u_h) + a(e,e) \tag{1.4}$$

Proof.

$$a(u,u) = a(u_h - e, u_h - e) = a(u_h,u_h) - 2a(u_h,e) + a(e,e) \tag{1.5}$$

and, by Galerkin orthogonality, we have $a(u_h,e) = 0$, since $u_h \in \mathcal{V}_h \underbrace{=}_{\text{by hypothesis}} \mathcal{V}_h^0$, which completes the proof. □

Corollary 1.2.4. *Error in energy and energy of the error From the previous theorem, we can write*

$$a(e,e) = a(u,u) - a(u_h,u_h) \tag{1.6}$$

The left hand side is the energy of the error. The right hand side is the error in energy (with a minus sign). This means that the energy of the error is $(-1)\times$ the error in energy.

Corollary 1.2.5. *Underestimation of the strain energy The finite element (strain) energy $a(u_h,u_h)$ is less than or equal to the exact (strain) energy $a(u,u)$.*

Proof. From the above,

$$\underbrace{a(u_h,u_h)}_{\text{finite element energy}} = \underbrace{a(u,u)}_{\text{exact energy}} - \underbrace{a(e,e)}_{\geq 0 \text{ by def. of } a} \tag{1.7}$$

thus,

$$a(u_h,u_h) \leq a(u,u) \tag{1.8}$$

□

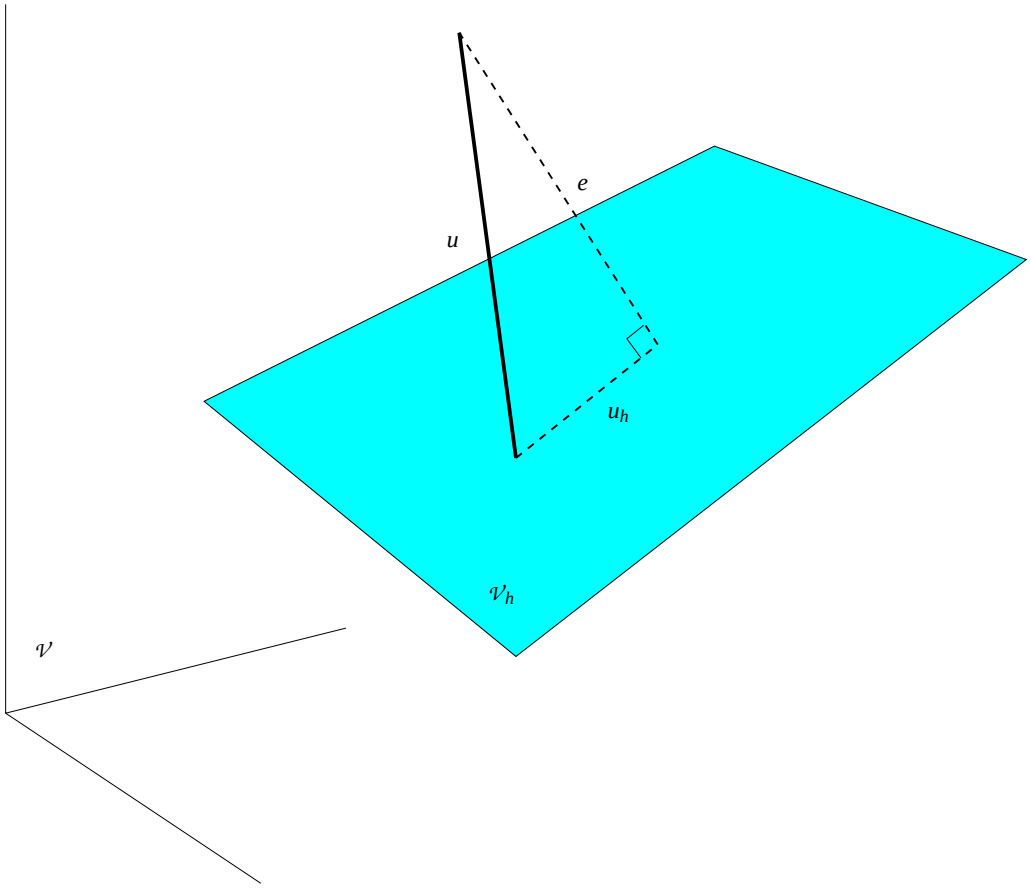

Figure 1.2: The orthogonal (with respect to bilinear form $a(\cdot,\cdot)$) projection of the exact solution u on the finite element space $\mathcal{V}_h \subset \mathcal{V}$ is the finite element solution u_h. On this figure, you can think of $e = u - u_h$ as a vectorial identity. In this figure, the space where the exact solution, u, lives is represented artificially as a three-dimensional space (in reality it is a space of infinite dimensions). The finite element subspace is a plane (dimension 2). The error, e is a member of $\mathcal{V}$, and the finite element solution a member of $\mathcal{V}_h$. Considering the right triangle in the figure, it can be immediately seen that the length of u (squared) equals the length of u_h (squared) plus the length of e, squared, i.e. $a(u,u) = a(u_h,u_h) + a(e,e)$ (Theorem 1.2.3). This identity is similar to the Pythagorean theorem in Euclidian spaces.

1.3 A priori error estimates in Sobolev Norms

Let Ω be an interval $]a,b[$ of $\mathbb{R}$,

Definition 1.3.1. *Continuity A function $f : \Omega \to \mathbb{R}$ is said to be of class $C^k(\Omega)$ (i.e. to be k times continuously differentiable) if and only if its k^{th} derivatives exist and are continuous functions.*

Definition 1.3.2. *Continuity and boundedness A function $f : \Omega \to \mathbb{R}$ is said to be bounded on $\Omega =]a,b[$ if and only if there exists a constant $c \in \mathbb{R}$ (independent on x), such that, for all $x \in]a,b[$, $|f(x)| < c$.*

Definition 1.3.3. *Continuity and boundedness A function $f : \Omega \to \mathbb{R}$ is said to be of class $C_b^k(\Omega)$ if and only if it is of class $C^k(\Omega)$ **and** is bounded on Ω.*

Definition 1.3.4. *Sobolev spaces A Sobolev space of degree k (known as H^k) is a set of functions with square-integrable[4] generalized derivatives until order k.*

For an elliptic problem defined on a domain Ω, the approximation error of a numerically robust and stable primal finite element analysis is known a priori (before the calculation is performed). Define the following:

- u: exact solution, assumed to possess r square integrable generalised derivatives.
- h: mesh size (diameter of the smallest circle containing the largest element in the mesh – Figure 1.3)
- p: polynomial order ($p \geq 1$) of the finite element approximation (linear shape functions: $p = 1$, quadratic shape functions: $p = 2$, etc.
- k: order of continuity of the "exact" solution (i.e. $u \in H^k(\Omega)$: u possesses k square integrable derivatives
- u^h: numerical (approximate) solution
- m is the highest order of derivatives appearing in the energy expression. For elasticity, $m = 1$ since the energy writes $\frac{1}{2}\int_\Omega \left(u_{i,j} + u_{j,i}\right) D_{ijkl} \left(u_{k,l} + u_{l,k}\right)$.
- $\|\cdot\|_m$ is the m^{th} Sobolev norm of function $\cdot$, i.e. the H^m norm of $\cdot$.

With these assumptions,

Theorem 1.3.1. *there exists a function $U_h \in \mathcal{V}_h$ and a constant c (independent of h, but dependent on p and u) such that*

$$\|u - U_h\|_m \leq c h^{\min(p+1-m, r-m)} \|u\|_r \tag{1.9}$$

It is almost a direct consequence that the error, e satisfies the following property

[4] square integrable functions are said to belong to the space L_2. They are also known as "L_2 functions".

Corollary 1.3.2. *Fundamental error estimate for elliptic boundary value problems there exists a constant $\bar{c}$ (independent of h, but dependent on p and u) such that*

$$\|e\|_m \leq \bar{c} h^{\min(p+1-m,r-m)} \|u\|_r \tag{1.10}$$

Proof. Let us compare $\|e\|_m$ and $\|u-U_h\|_m$. Since $\|\cdot\|_m$ and $a(\cdot,\cdot)$ are equivalent norms, we can find a constant $c_1 \in \mathbb{R}$ such that

$$\|e\|_m \leq \frac{1}{c_1} a(e,e)^{\frac{1}{2}}. \tag{1.11}$$

But u_h is the best approximation to u in the sense of a (Theorem 1.2.2), therefore, for any $U_h \in \mathcal{V}_h^0$,

$$\frac{1}{c_1} a(e,e)^{\frac{1}{2}} \leq \frac{1}{c_1} a(u-U_h, u-U_h)^{\frac{1}{2}}. \tag{1.12}$$

Using again the equivalence of $\|\cdot\|_m$ and $a(\cdot,\cdot)$, we can find a constant $c_2 \in \mathbb{R}$ such that

$$a(u-U_h, u-U_h)^{\frac{1}{2}} \leq c_2 \|u-U_h\|_m. \tag{1.13}$$

Combining this equation with (1.12) and (1.11), we obtain

$$\|e\|_m \leq \frac{c_2}{c_1} \|u-U_h\|_m \tag{1.14}$$

Letting $\bar{c} = \frac{c_2}{c_1}$ and using the result of Theorem 1.3.1 we obtain the desired result.

□

Let us examine (1.10). First, recall that we wish the left hand side to be as small as possible (to minimise the error). If the right hand side is small, the H^m norm $\|e\|_m$ of the error, e, is blocked between 0 and a small number and, consequently, also has to be small.

Let us see various possibilities to decrease the magnitude of the right hand side.

Let us first note that for the method to be convergent, we must have

$$\min(p+1-m, r-m) > 0 \tag{1.15}$$

otherwise, the right hand side of (1.10) would not go to zero as $h \to 0$ (it would go to infinity). The condition $\min p+1-m, r-m > 0$ can be rewritten

$$p+1-m > 0 \quad \text{and} \quad r-m > 0, \tag{1.16}$$

equivalently:

$$p > m-1 \quad \text{and} \quad r > m. \tag{1.17}$$

Theorem 1.3.3. *In words, this means that in order for the finite element method to converge optimally in norm $\|\cdot\|_m$ we must*

- *select the polynomial order p larger than $m-1$*
- *make sure that the exact solution, u is such that it is more regular than the order of norm $\|\cdot\|_m$*

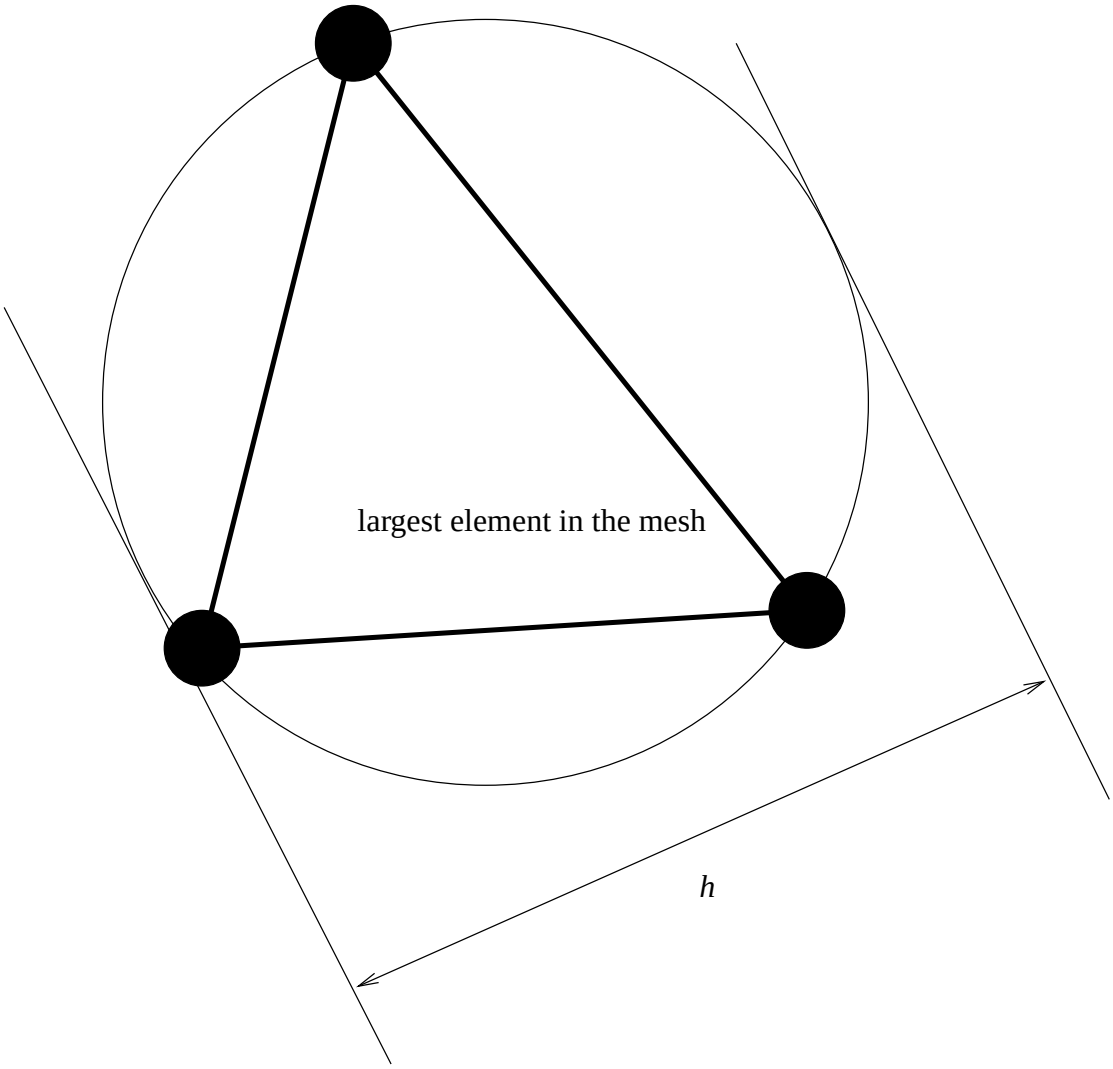

Figure 1.3: The mesh size, h is the diameter of the smallest circle enclosing the largest element in the mesh.

Theorem 1.3.4. *If u is in H^{p+1} (then $r = p+1$) and the error expression becomes*

$$\|e\|_m \leq \bar{c}h^{\min(p+1-m,r-m)}\|u\|_r = \bar{c}h^{\min(p+1-m,p+1-m)}\|u\|_{p+1} = \bar{c}h^{p+1-m}\|u\|_{p+1} \tag{1.18}$$

Example 1.3.1. *Elasticity For elasticity, we have $m = 1$ (only the first derivative of the displacement u appears in the energy expression). If we measure the error in the H^1 norm (also known as energy norm), then $m = 1$. If we further assume that the solution u is in H^{p+1}, as in Theorem 1.3.4, we can use Equation (1.18), which becomes*

$$\|e\|_1 \underbrace{\equiv}_{def} \|e\|_{H^1} \leq \bar{c}h^{p+1-1}\|u\|_{p+1} = \bar{c}h^p\|u\|_{p+1} \tag{1.19}$$

One conclusion that we can draw from Equation (1.19), is that when the exact solution u is smooth enough (in H^{p+1}, the convergence rate of the H^1 norm of the finite element error can be increased by two techniques:

- *decreasing h (this is known as h-adaptivity), i.e. decreasing the element size*
- *increasing p (this is known as p-adaptivity), i.e. increasing the polynomial order used in the approximation*

However, these techniques are not always successful. Let us go back to the error bound:

$$\|e\|_m \leq \bar{c}h^{\min(p+1-m,r-m)}\|u\|_r \tag{1.20}$$

Looking at the exponent, we note that if the regularity r of the exact solution is low, there is no use increasing the polynomial order p, because $r-m$ will remain the determining term in $\min(p+1-m, r-m)$. This is why, if the exact solution is "rough" (i.e. has a low order of continuity), the standard finite element method is not well-suited, in general, and needs to be improved. An improvement of this method is the extended finite element method (XFEM), notions of which will be given in Section "Enriched Methods."

1.4 Conclusions

In this chapter, we discussed the various sources of error in numerical simulation, from setting up the problem, to its numerical solution. We looked at a priori error estimation, which gives us, before carrying out a calculation, an upper bound (maximum value) for the error. We saw that the Galerkin FE solution is optimal in the sense of the bilinear form defining the boundary value problem, and we learnt that the error of the finite element solution is governed by the degree of continuity of the exact solution to be approximated, the polynomial order of the approximation, the mesh size, and the norm used to measure the error. We discovered that the FEM is not well-suited to solve problems with rough solutions (see Enriched Methods part of the course).

In the following chapter, we will start looking at techniques to measure the error a posteriori, and briefly compare them.

Chapter 2

Some methods to measure the approximation error

2.1 Existing a posteriori error estimation techniques

Why do we resort to numerical methods? Usually, the problems we are to solve are too complex for us to derive closed-form solutions analytically. The problem is discretised and solved numerically. The major challenge in estimating the approximation error committed by the numerical method of choice emanates from the obvious fact that the numerical solution may not be compared to an analytical solution, since the latter is unknown.

Two routes have emerged from error estimation research to solve this difficulty: *recovery* and *residual* based a posteriori error estimates.

Recovery based error estimation consists in constructing an *enhanced* solution from a suitable transformation (usually smoothing) of the numerical (raw) solution, with the objective to employ this improved solution as a substitute for the unknown exact solution. An obvious requirement for this enhanced solution is that it be closer to the exact solution than the raw solution.

To understand residual based error estimators, let us consider, to fix ideas, the simple case of static solid mechanics, where the problem is to find the stress field in the body such that the latter is in equilibrium with the external forces. Assume that the standard FEM is used to solve this problem numerically. Residual based error estimators seek the error by measuring, in each finite element, how far the numerical stress field is from equilibrium and, consequently, do not require the construction of an enhanced solution.

A remarkable and often disconcerting feature of recovery based error estimation is that with *no additional information than that available in the raw numerical solution*, an enhanced solution can be built and, by comparing it to the raw solution, the error can be estimated.

In general, the estimated error does not equal the exact error. For recovery estimators, this is because the enhanced solution does not equal the exact solution. In residual estimation, the computation of the residual itself must be estimated using a numerical method (usually the same as the original one being assessed), leading to an additional source of error.

A point in favour of recovery based estimators is that the ratio of the estimated error to the exact error (known as the *effectivity*) is close to unity. On the other hand, residual based estimators are usually less effective, but can provide mathematical *error bounds*, which, in certain cases can be very useful, since they prove that the estimated error is larger than the exact error. Unfortunately, these bounds may include constants which are often very difficult to evaluate in practice: probably the

major reason for industry's preference for residual based error estimates.

The interested reader can refer to the well-known review article of Professor Ainsworth [1].

2.2 Recovery based error estimation

A posteriori error estimation has the difficult task to measure the error committed by a numerical solution without knowing what the exact solution is. The basic idea of recovery based error estimation, is to construct, with only the information contained into the numerical solution, an enhanced solution that will play the role of the exact solution. The error is then defined by the difference between this improved solution (enhanced solution) and the initially obtained numerical solution (raw solution). This technique was invented by Professor Zienkiewicz and are reported in his famous papers [30–32].

There are several techniques that can be used to obtain the enhanced solution. One of the simplest one is smoothing. The basic idea is depicted in Figure 2.2, which shows the original solution (piecewise constant), the improved solution (bold piecewise linear line) and the exact solution (dashed curve). Notice that the improved solution approximates the exact solution much better than the original "stair-case" solution. In order to improve the accuracy of the enhanced solution, the nodal stress (strain) fiels can be computed from the stress/strain fields of the neighbouring elements, evaluated at so-called "superconvergent points." These points were discovered by Barlow (Figure 2.2), and are the points in the element where the derivatives (strain, stress) are most accurate.

The notion of smoothing, or derivative recovery was extended by Bordas and Duflot to enriched finite element approximations (See Chapter 4, Figures 4.1 and 4.2). On these figures, you can see the "stair-casing" present in the raw solution, which is suppressed by smoothing. See also References [10–13, 29].

The smoothing scheme presented in Figure 2.2 is very simple, and many improvements have been proposed (see [1] for details). A simple improvement would be to express the smoothed stress (strain) field at each node as the average of the stress (strain) evaluated at the superconvergent point (Barlow point) of the two neighbouring elements, weighted by the length of the element.

Error estimates based on smoothing techniques are widely used in the engineering community (for example, the commercial code UGS/EDS-PLM I-DEAS has mesh-adaption capability for linear elasticity problems as well as plate and shell formulations).

The assumption of superconvergence is not required for these methods to work, and it is possible to show that averaging (smoothing) based error estimates tend to overestimate the error (which is important for engineering applications).

If the superconvergence property is satisfied, it is possible to show that certain classes of averaging error estimates are asymptotically exact (when the mesh size, h goes to zero).

2.3 Explicit residual based error estimation techniques

These estimators, known as "explicit" (see Ainsworth [1]), because the sole knowledge of the approximate solution suffices to evaluate them.

The general idea is to measure how accurately the boundary value problem is solved in each element. Let us imagine we are solving an elasticity problem. The boundary of the domain is split into two non-overlapping parts: the Dirichlet and the Neumann boundaries. There will therefore be three categories of elements: interior elements (for which no node lies on the boundary); Dirichlet elements (for which at least one node lies on the boundary) and Neumann elements for which at least

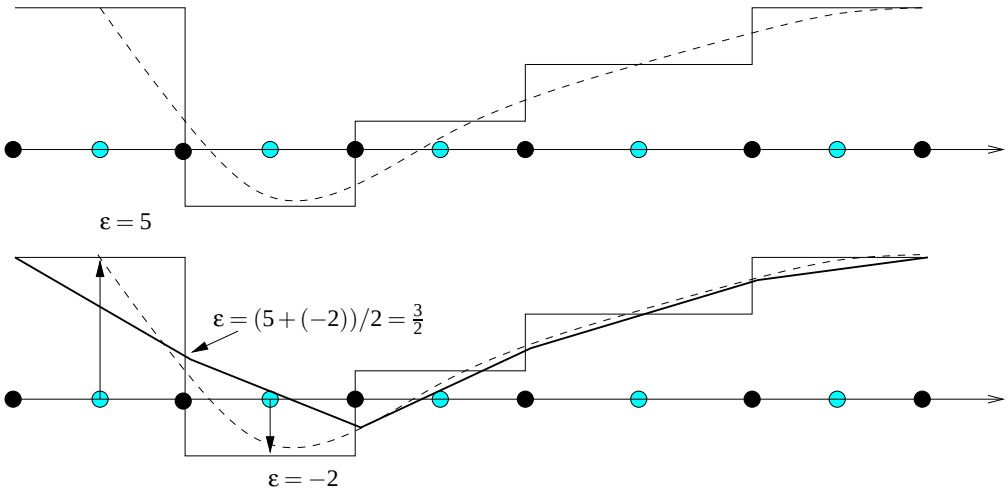

Figure 2.1: Superconvergent Patch Recovery (SPR). Original (raw), improved (enhanced) and exact solution for linear 1D elements. For an elasticity problem, the field shown could be the stress or strain field, i.e. the fields obtained by differentiating the displacement solution. At each node, the enhanced solution is constructed as the average of the stress (strain) value in the neighbouring elements.

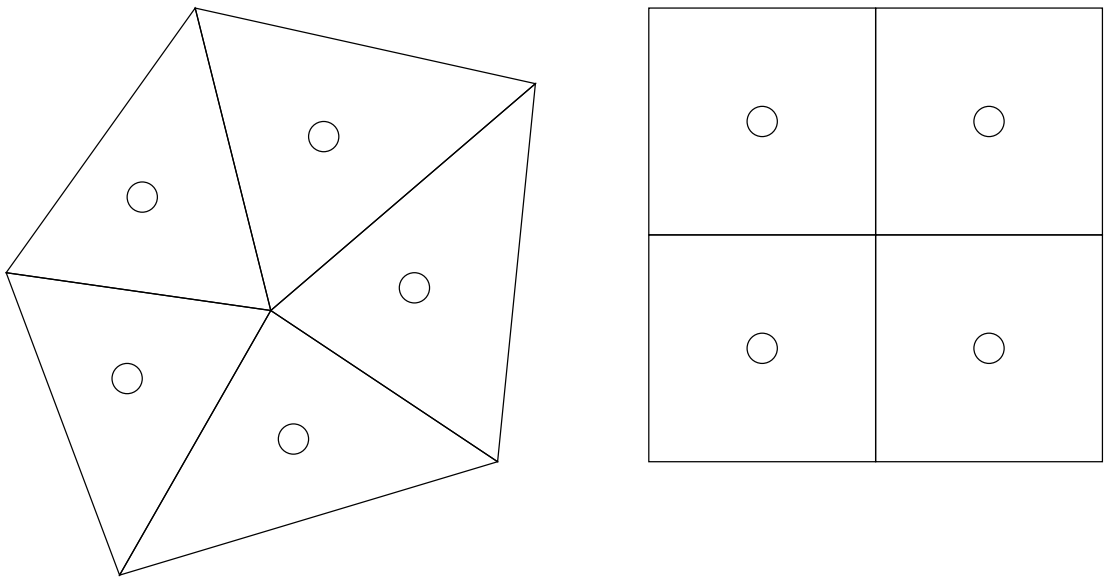

linear triangles ($p = 1$)

linear quadrangles ($p = 1$)

Figure 2.2: Barlow (superconvergent) points for linear triangular elements and bilinear quadrilateral elements are located at the centre of the elements.

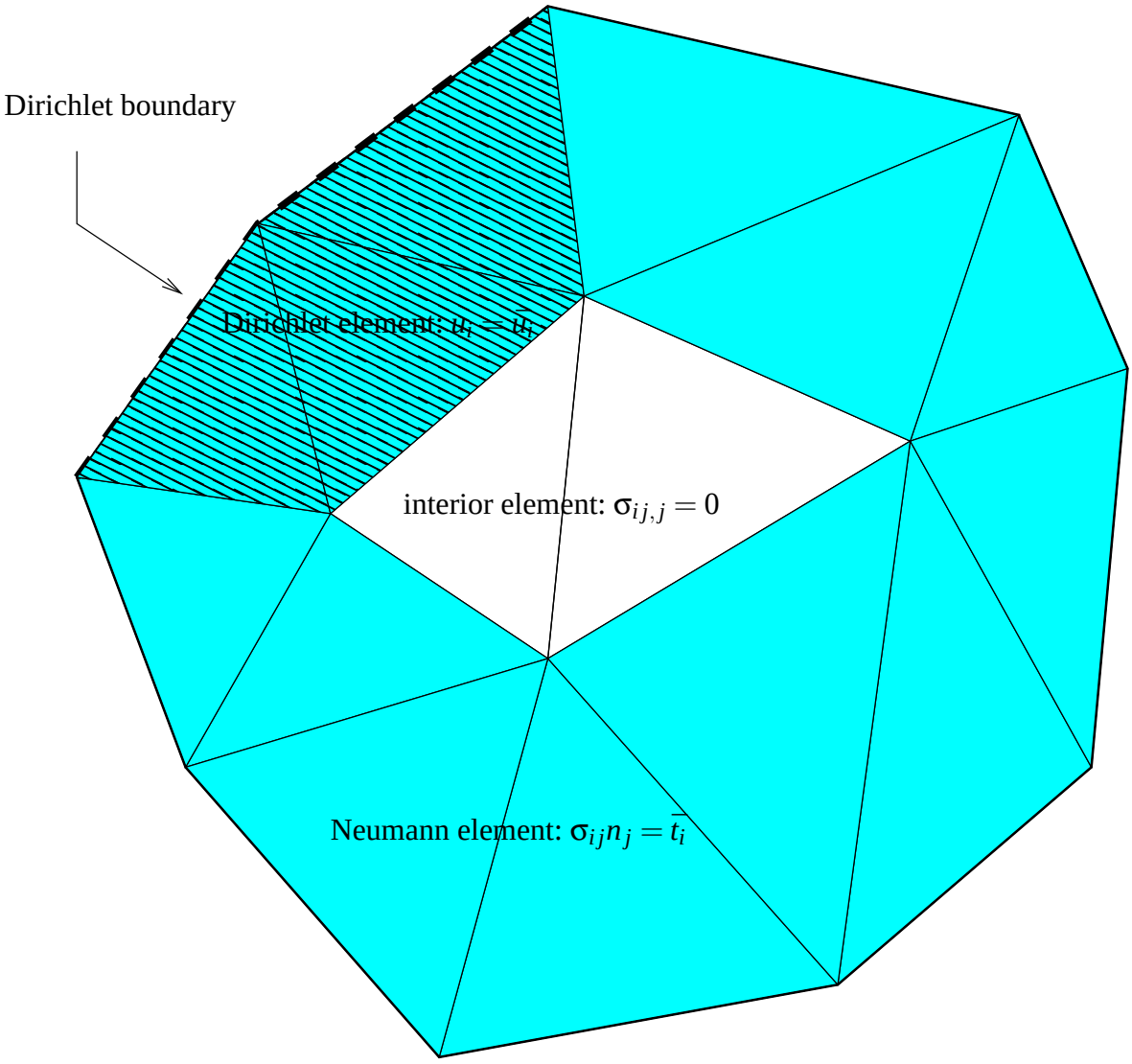

Figure 2.3: Element categories for residual based error estimators.

one node lies on the Neumann boundary. There will also be some mixed elements, for which some nodes are on the Neumann boundary, and other nodes on the Dirichlet boundary.

For each of these element categories, the residual (difference between the solution and the equilibrium) will be computed in a different way. For interior elements, the equilibrium condition must be verified ($\sigma_{ij,j} = 0$), for Neumann boundaries, the surface tractions must equal the imposed tractions ($\sigma_{ij} n_j = \bar{t}_i$), and for the Dirichlet boundary, the imposed displacements must equal the imposed displacements ($u_i = \bar{u}_i$). The basic idea is shown in Figures 2.3 and 2.3.

Explicit error estimators lead to local error indicators, including unknown (usually) constants. It is possible to find bounds for these constants, but these bounds are usually such that the error estimator is pessimistic.

Additionally, to measure the global error, we need to give a weight to each type of residual, depicted in Figures 2.3 and 2.3. Choosing these weights is not obvious.

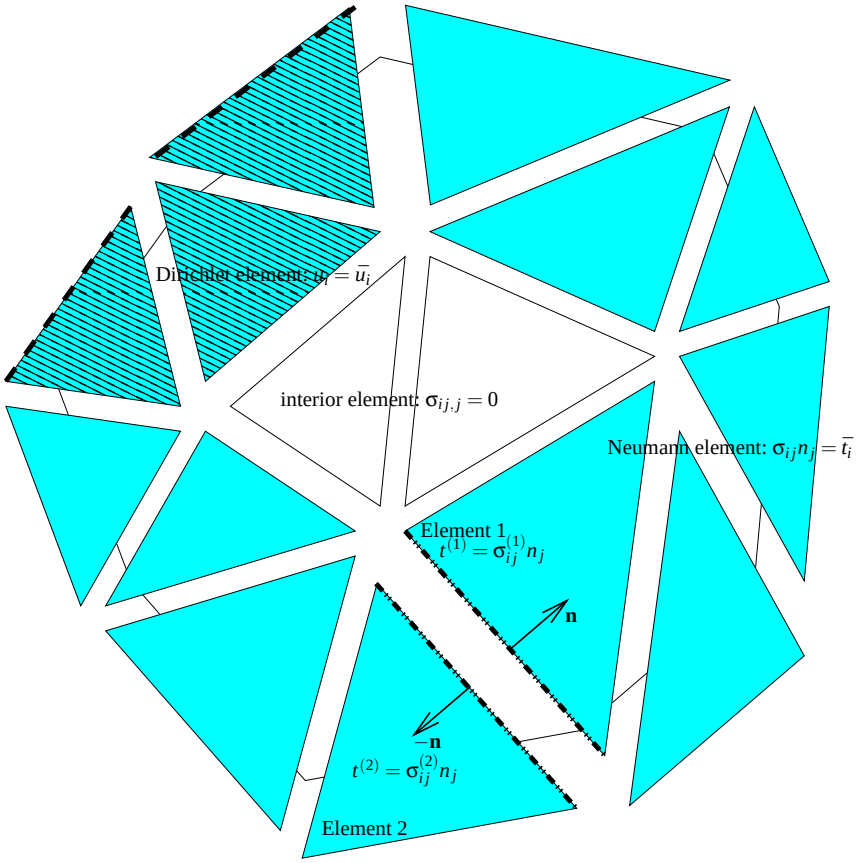

Figure 2.4: Element categories for residual based error estimators. Note that the stress continuity through the element boundaries is part of the residuals to be computed.

2.4 Implicit residual base error estimation techniques

Implicit error estimation techniques require the solution of a local (in each element or over a small group of elements) boundary value problem approximating the equation for the error itself. An estimate of the error is then taken as the norm of the solution to this local boundary value problem.

In implicit error estimators, an auxiliary boundary value problem, with the residual as data is used. This suppresses the difficulty associated with the relative weighting of the residuals (see Section 2.3). However, a disadvantage of this technique is that it requires solving an additional boundary value problem numerically, which implies the choice of a suitable approximation scheme. This can be problematic. Examples of implicit residual methods are:

- the element residual method;
- the subdomain residual method.

The interested reader is referred to the review paper by Ainsworth and Oden [1] and Ainsworth's book [2].

2.5 Measuring the adequacy of an error estimator

For simplicity, we restrict here to recovery-based error estimates. Let Ω_q be an element in the mesh, the *error* between the raw and the smoothed solution can be measured by the norm

$$e^{hs}_{\Omega_q} = \sqrt{\int_{\Omega_q} \left\| \varepsilon^h(\mathbf{x}) - \varepsilon^s(\mathbf{x}) \right\|^2 d\mathbf{x}}. \tag{2.1}$$

Since the enhanced solution is different from the exact solution, this measure is only an *approximate error*. The global approximate error is measured by the sum of the elemental errors on the n_{elt} elements of the mesh

$$e^{hs} = \sqrt{\sum_{q=1}^{n_{elt}} {e^{hs}_{\Omega_q}}^2}. \tag{2.2}$$

We then define $e^{he}_{\Omega_q}$ as the following error norm between the raw XFEM solution and the exact solution on element Ω_q

$$e^{he}_{\Omega_q} = \sqrt{\int_{\Omega_q} \left\| \varepsilon^h(\mathbf{x}) - \varepsilon^{exact}(\mathbf{x}) \right\|^2 d\mathbf{x}}, \tag{2.3}$$

and we call this error measure the *exact error* since it measures the distance between the raw XFEM solution and the exact solution. Summing over the elements in the mesh, the global exact error writes

$$e^{he} = \sqrt{\sum_{q=1}^{n_{elt}} {e^{he}_{\Omega_q}}^2}. \tag{2.4}$$

The *effectivity index* of the error estimator is defined as the *ratio of the approximate error to the exact error*

$$\theta = \frac{e^{hs}}{e^{he}}. \tag{2.5}$$

A good estimator has an *effectivity close to unity*, which means that the measured (approximate) error is close to the exact error. In other words, the enhanced solution is close to the exact solution.

2.6 Adaptivity or what to do with the error distribution?

The techniques presented briefly above permit the calculation, for all elements in the mesh, of the elemental contribution to the global error. In practice, an engineer wants to limit both the global and the element-wise error. The error estimators produce error maps, on the whole mesh, similar to Figure 2.6. In 2.6, *p* adaptivity, in the region of highest error, is shown. Additional (mid-side) nodes are required to support the higher order shape functions. An example of *h* adaptivity is shown in Figure 2.6 and a typical approximation adaptation cycle is shown in Figure 2.8.

2.7 Conclusions

In this chapter, we learnt how to measure, a posteriori (after the calculations are finished), the error of a numerical approximation. We learnt about explicit and implicit error estimates as well as smoothing (recovery) based and residual based estimates and compared them succintly. We also discussed possibilities to measure the effectivity of an error estimator.

In the next chapter, we will focus on goal-oriented error estimation, which is useful when the quantity of interest is not only the global strain energy, but, possibly, the average stress in a given subregion of a component, or, as is the case in fracture mechanics, the value of the crack driving force, i.e. the stress intensity factor or more generally, the energy release rate.

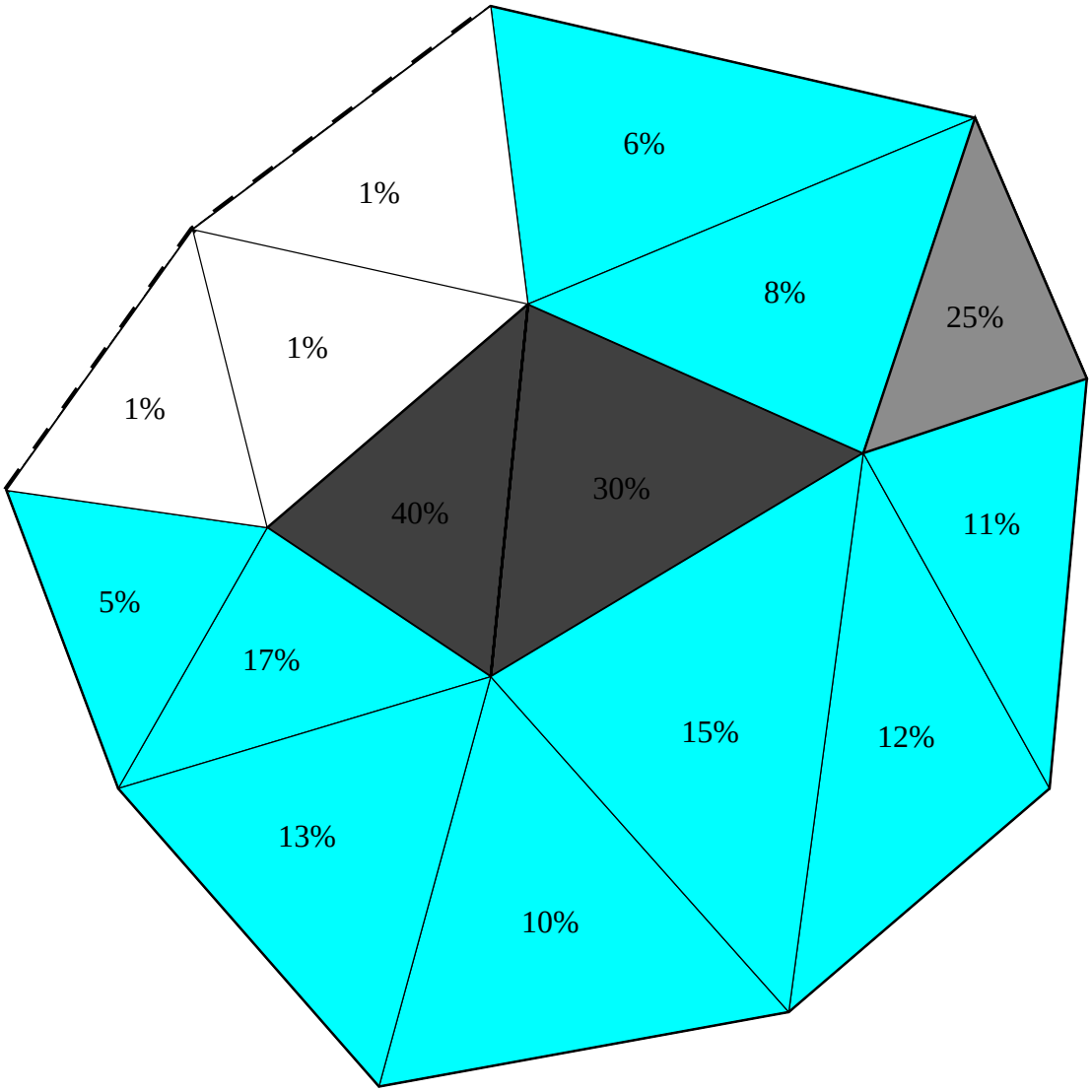

Figure 2.5: Error map. The darkest elements have the highest error. These elements can theb be subdivided (*h* refinement), the polynomial order can be increased in these elements (*p* refinement – beware! We saw in Chapter 3.1 that this was useless for low-continuity exact solutions such as linear elastic fracture mechanics or other singular solutions. Alternatively, nodes can be moved around without increasing the number of elements, nor changing the approximation order (relocation adaptivity: *r*-adaptivity). Figure provided for example purposes only, it is unlikely that an error distribution looks like this for a real approximation.

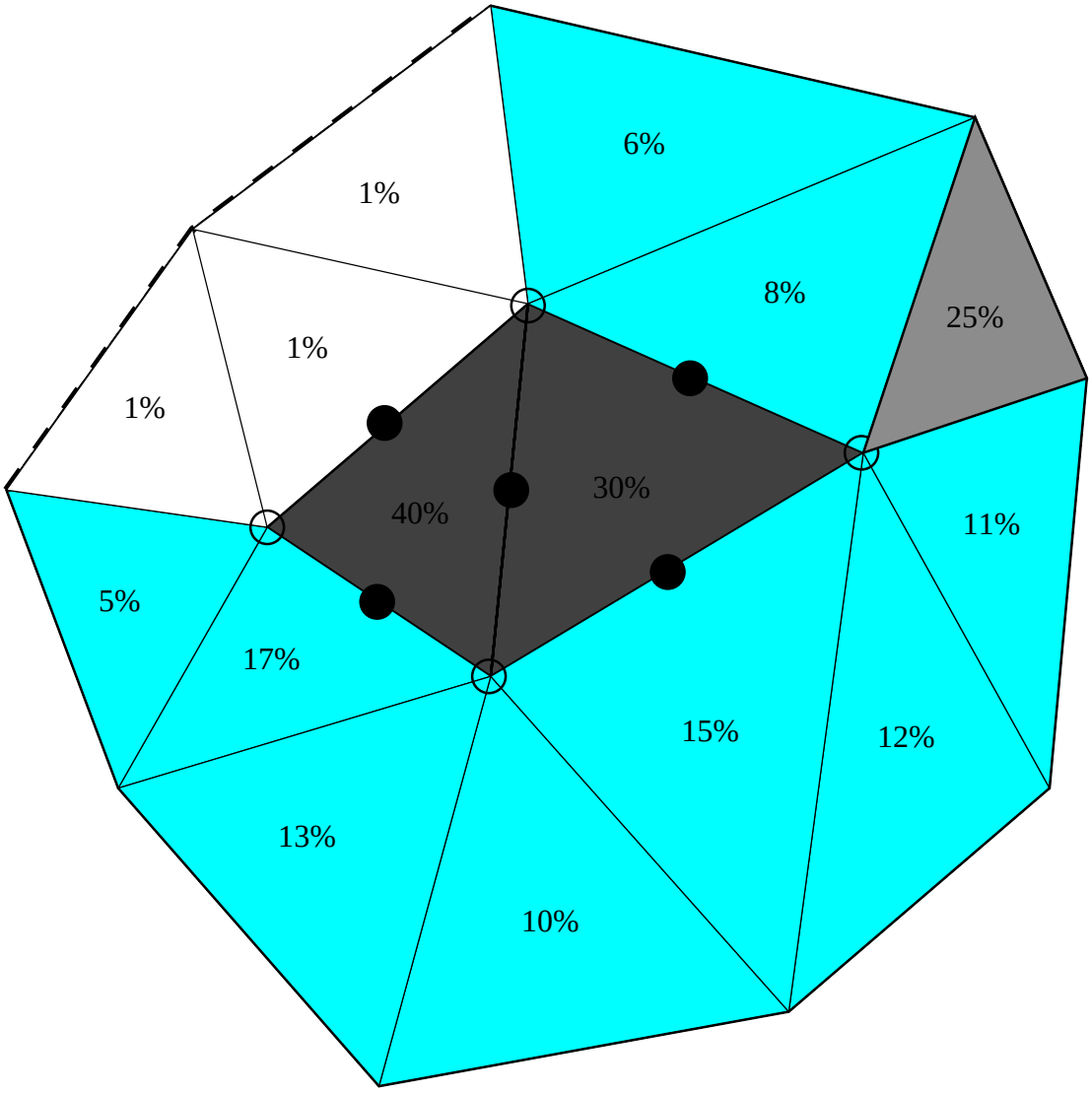

nodes present before *p* adaptivity

additional nodes used to increase the polynomial order, *p*

Figure 2.6: A simple example of *p* adaptivity in the region of highest error

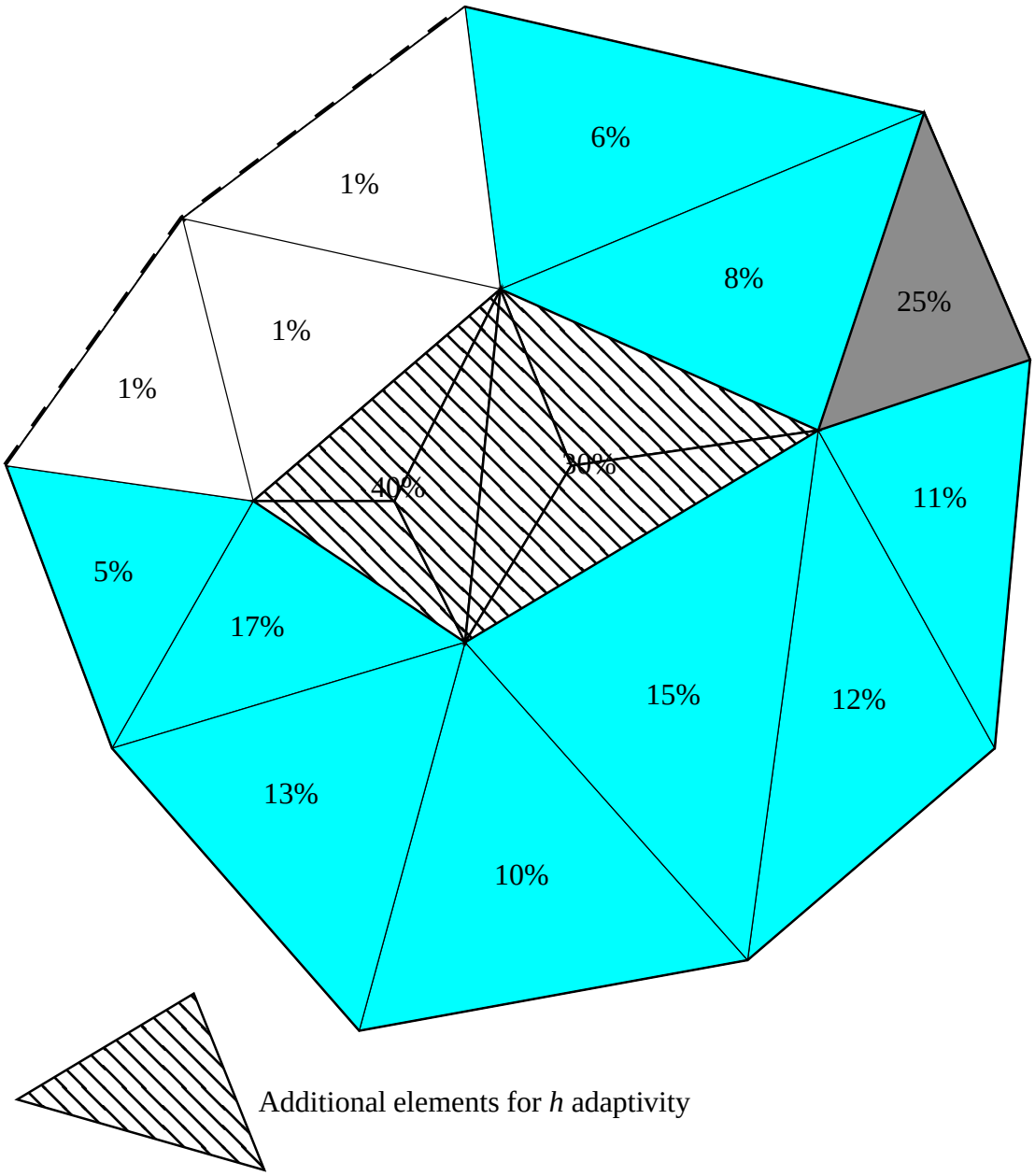

Figure 2.7: A simple example of *h* adaptivity in the region of highest error

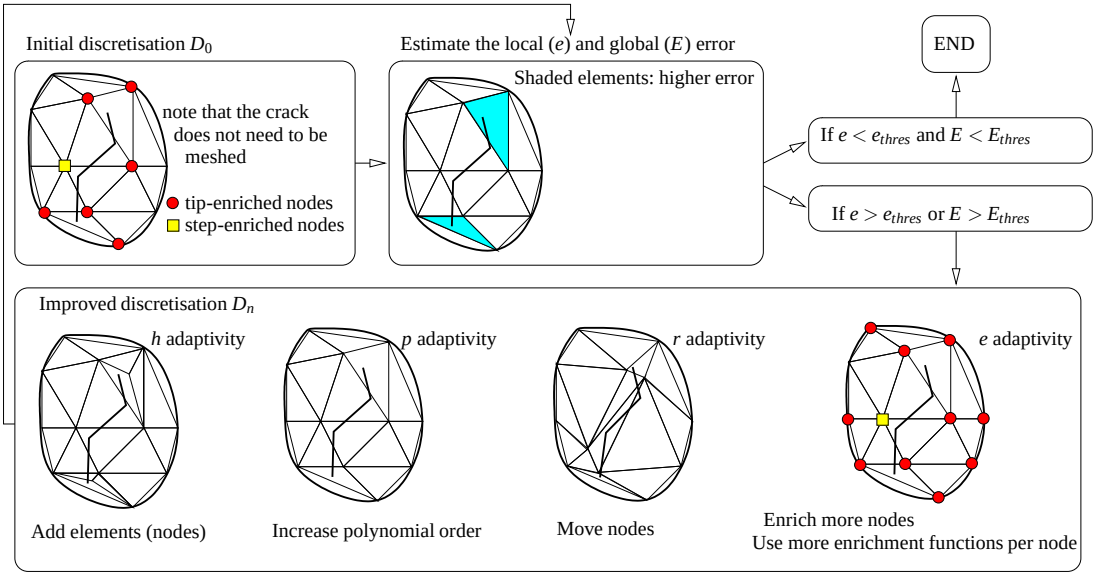

Figure 2.8: Adaptivity, a schematic explanation.

This page intentionally contains only this sentence.

Chapter 3

First notions on goal-oriented error estimation

3.1 Introduction

In linear elastic fracture mechanics (LEFM), the main quantity of interest is the energy release rate G along the front (tip) of the cracks. Domain forms of interaction energy integrals [20] are well suited to the computation of the stress intensity factors required to compute G. One can therefore argue that it is the error on G committed by the numerical approximation that should be measured, as opposed to the traditional error on the energy.

Goal-oriented a posteriori error estimates are well-established techniques to help measure and control the *local* error on a (non)linear functional of interest.

3.2 LEFM problem statement and extended finite element discretization

3.2.1 LEFM problem

To begin with, we briefly present the linearized elasticity problem. Therefore, let us first introduce the isotropic elastic body which is given by the closure of a bounded open set $\Omega \subset \mathbb{R}^3$ with a piecewise smooth and polyhedral boundary Γ such that $\Gamma = \overline{\Gamma}_D \cup \overline{\Gamma}_N$ and $\Gamma_D \cap \Gamma_N = \emptyset$, where Γ_D and Γ_N are the portions of the boundary Γ where Dirichlet and Neumann boundary conditions are imposed, respectively. Assuming, for the sake of simplicity, homogeneous Dirichlet boundary conditions, all admissible displacements $\mathbf{u} : \overline{\Omega} \to \mathbb{R}$ of the elastic body $\overline{\Omega}$ are elements of the Hilbert space $\mathcal{V} = \{\mathbf{v} \in [H^1(\Omega)]^3 \,;\, \mathbf{v}|_{\Gamma_D} = 0\}$.

The weak formulation of the linearized elasticity problem—which is also termed the primal problem throughout this paper—then reads: find $\mathbf{u} \in \mathcal{V}$ such that

$$a(\mathbf{u}, \mathbf{v}) = F(\mathbf{v}) \quad \forall \mathbf{v} \in \mathcal{V} \tag{3.1}$$

with the continuous, symmetric and $\mathcal{V}$-elliptic bilinear form $a : \mathcal{V} \times \mathcal{V} \to \mathbb{R}$ and the continuous linear form $F : \mathcal{V} \to \mathbb{R}$ defined by

$$a(\mathbf{u}, \mathbf{v}) = \int_\Omega \boldsymbol{\sigma}(\mathbf{u}) : \boldsymbol{\varepsilon}(\mathbf{v}) dV \tag{3.2}$$

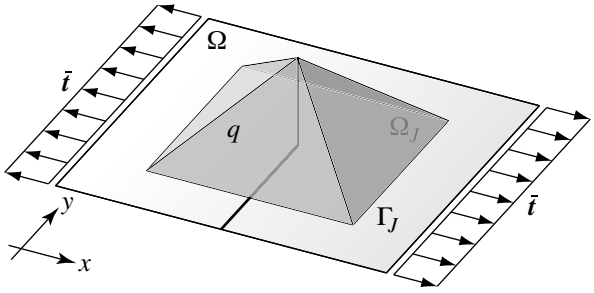

Figure 3.1: Pre-cracked specimen, boundary conditions and q-function as a pyramid function.

and

$$F(\mathbf{v}) = \int_{\Gamma_N} \bar{\mathbf{t}} \cdot \mathbf{v} dA, \tag{3.3}$$

respectively. Here, $\sigma = \mathbf{C} : \varepsilon$ denotes the stress tensor given in terms of the fourth-order elasticity tensor $\mathbf{C}$ and the second-order strain tensor ε defined as the symmetric gradient of $\mathbf{u}$. Furthermore, $\bar{\mathbf{t}} \in [L_2(\Gamma_N)]^3$ are prescribed tractions imposed on the Neumann boundary Γ_N. For the sake of simplicity, body forces are omitted in the above formulation.

3.2.2 The J-integral as a crack propagation criterion

As mentioned earlier, in LEFM the energy release rate and the J-integral concept are equivalent. The J-integral, which is a nonlinear functional $J : \mathcal{V} \to \mathbb{R}$, can be derived by a straightforward application of the concept of material forces, see, e.g., Steinmann et al. [26], since J is the projection of the material force $\mathbf{F}_{mat}$ acting on the crack tip into the direction of crack propagation (given in terms of the unit vector $\mathbf{e}_{||}$ which is a priori known in this paper due to symmetry conditions with respect to both the boundary conditions and the geometry of the elastic body). It is computationally convenient to use the domain expression of J, as introduced by Shih et al. [25], which then reads

$$J(\mathbf{u}) = \mathbf{F}_{mat} \cdot \mathbf{e}_{||} = -\int_{\Omega_J} \mathbf{H}(q\mathbf{e}_{||}) : \tilde{\Sigma}(\mathbf{u}) dV. \tag{3.4}$$

Here, $q = q(x,y)$ (or $q = q(x,y,z)$ in three space dimensions) represents an arbitrary, piecewise continuously differentiable weighting function with $q = 1$ at the crack tip and $q = 0$ on the contour (or surface) Γ_J that bounds the area (or volume) Ω_J. For example, q can be conveniently chosen as a pyramid function as shown in Figure 3.1. Furthermore, $\tilde{\Sigma}$ denotes the so-called Newton-Eshelby stress tensor given by

$$\tilde{\Sigma} = W_s \mathbf{I} - \mathbf{H}^T \cdot \sigma \tag{3.5}$$

with specific strain-energy function W_s, second-order identity tensor $\mathbf{I}$ and displacement gradient $\mathbf{H} = \nabla\mathbf{u}$. Assuming that $\mathbf{e}_{||} = (10)^T$, the classical form of the J-integral can be easily obtained.

A pre-existing crack then starts to grow in the direction of $\mathbf{e}_{||}$ if J exceeds the (known) material dependent threshold J_c.

3.2.3 Definitions

In what follows, the following definitions are assumed:

- $\mathcal{V}$ is the exact test space

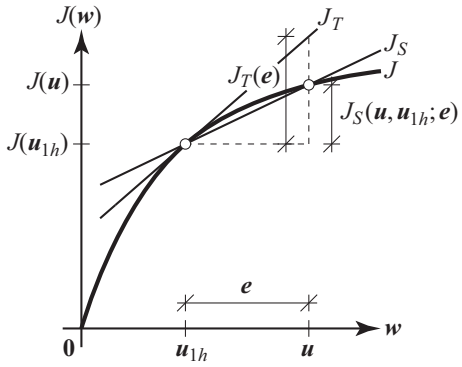

Figure 3.2: Schematic visualization of the linearizations of the J-integral.

- $\mathbf{u} \in \mathcal{V}$ is the exact solution to the exact crack problem and $\mathbf{v} \in \mathcal{V}$ is a test function.

The bilinear form $a : \mathcal{V} \times \mathcal{V} \to \mathbb{R}$ and the linear functional $F : \mathcal{V} \to \mathbb{R}$ were defined in 3.2 for the linear elasticity model problem. The variational equation for $\mathbf{u}$ is

$$\text{Find } \mathbf{u} \in \mathcal{V} \mid \forall \mathbf{v} \in \mathcal{V} \quad a(\mathbf{u}, \mathbf{v}) = F(\mathbf{v}) \tag{3.6}$$

The discretized version of the variational principle restricts the problem to seeking a solution $\mathbf{u}_h$ in a finite-dimensional subspace of $\mathcal{V}_h \subset \mathcal{V}$ and writes

$$\text{Find } \mathbf{u}_h \in \mathcal{V}_h \mid \forall \mathbf{v}_h \in \mathcal{V}_h \quad a(\mathbf{u}_h, \mathbf{v}_h) = F(\mathbf{v}_h) \tag{3.7}$$

The Lax-Milgram theorem guarantees existence and uniqueness of a solution for both variational problems (3.6) and (3.7).

Obviously, the discretized version of the variational principle yields a solution $\mathbf{u}_h$ which is not exact, and we note $\mathbf{e}_\mathbf{u} = \mathbf{u} - \mathbf{u}_h$ the discretization error.[1]

3.3 Goal-oriented error estimate

Our goal is now to evaluate the discretization error on the non-linear functional $J : \mathcal{V} \to \mathbb{R}$ defined in 3.2.2 committed upon discretization of the variational problem, i.e. we seek an estimate of the quantity $J(\mathbf{u}) - J(\mathbf{u}_h)$, which is our *goal-oriented error measure*. This error measure, however, is non-linear by definition. Therefore, as shown in Rüter and Stein [23] based on the seminal work by Eriksson et al. [14] and Becker and Rannacher [8], we first need to linearize the J-integral[2]

which results in the following expression

$$J(\mathbf{u}) - J(\mathbf{u}_h) = J_S(\mathbf{u}, \mathbf{u}_h; \mathbf{e}_\mathbf{u}) \tag{3.8}$$

with secant form $J_S : \mathcal{V} \to \mathbb{R}$, defined as

$$J_S(\mathbf{u}, \mathbf{u}_h; \mathbf{v}) = \int_0^1 J'(\xi(s); \mathbf{v}) ds, \tag{3.9}$$

[1] The subtraction is well defined since we proved earlier that $\mathcal{V}_h \subset \mathcal{V}$ and hence, subtracting $\mathbf{u}_h$ from $\mathbf{u}$ is permitted.

[2] we note that an *exact linearization*, which is a secant form, $J_S(\mathbf{u}, \mathbf{u}_h; \mathbf{e}_\mathbf{u})$, of J, involves the (unknown) exact solution $\mathbf{u}$ and is therefore not computable. We therefore fashion an *approximate linearization*, a tangent linearization of J, as the linear functional $J_T(\cdot)$ obtained by setting $\mathbf{u} = \mathbf{u}_h$ in J_S (3.2)

see [23]. In the above, the tangent form of J is defined as

$$J'(\xi(s);\mathbf{e_u}) = D_u J(\mathbf{u})|_\xi(s)\cdot\mathbf{e_u}, \tag{3.10}$$

that is the Gâteaux derivative of J with respect to $\mathbf{u}$ in the direction of the discretization error $\mathbf{e_u}$ and $\xi(s) = \mathbf{u}_h + s\mathbf{e_u}$, $s\in[0,1]$.

Since the linearization J_S involves the (generally unknown) exact solution $\mathbf{u}$, we next introduce a computable approximation J_T of J_S by replacing the exact solution $\mathbf{u}$ with the (known) finite element solution $\mathbf{u}_h$. Hence, we arrive at the tangent form

$$J_T(\cdot) = J'(\mathbf{u}_h;\cdot) = J_S(\mathbf{u}_h,\mathbf{u}_h;\cdot) \approx J_S(\mathbf{u},\mathbf{u}^h;\cdot) \tag{3.11}$$

that holds for small errors $\mathbf{e_u}$ only. A schematic visualization of the derivations presented above can be seen in Figure 3.2.

With the above definition at hand, the exact linearization of (3.4) yields

$$J_S(\mathbf{u},\mathbf{u}_h;\mathbf{v}) = -\int_0^1\int_{\Omega_J}\mathbf{H}(q\mathbf{e}_{||}) : C_\Sigma(\xi(s)) : \mathbf{H}(\mathbf{v})dVds, \tag{3.12}$$

whereas the associated tangent form J_T is given by

$$J_T(\mathbf{v}) = -\int_{\Omega_J}\mathbf{H}(q\mathbf{e}_{||}) : C_\Sigma(\mathbf{u}_{1h}) : \mathbf{H}(\mathbf{v})dV. \tag{3.13}$$

In the above, C_Σ denotes the fourth-order tensor of elastic tangent moduli associated with the Newton-Eshelby stress tensor defined as

$$C_\Sigma = \frac{\partial\tilde{\Sigma}}{\partial\mathbf{H}} = \mathbf{I}\otimes\sigma - \mathbf{I}\underline{\otimes}\sigma - \mathbf{H}^{\mathbf{T}}\cdot\mathbf{C}, \tag{3.14}$$

see Heintz et al. [16]. Here, "$\underline{\otimes}$" denotes a non-standard dyadic product operator. For further elaborations on the linearizations of the domain as well as the contour expression of the J-integral we refer to Rüter and Stein [23].

$$\begin{aligned} J_T(\cdot) &= J'(\mathbf{u}_h;\cdot) && (3.15)\\ &= J_S(\mathbf{u}_h,\mathbf{u}_h;\cdot) && (3.16)\\ &\approx J_S(\mathbf{u},\mathbf{u}_h;\cdot) && (3.17)\end{aligned}$$

3.3.1 Duality techniques

We have now derived an approximation, J_T for the discretization error $J(\mathbf{u}) - J(\mathbf{u}_h)$ committed on the J integral. How can this error be computed? We follow the strategy of solving an *auxiliary dual problem*, which we define next. Let us introduce the bilinear form $a^* : \mathcal{V}\times\mathcal{V}\to\mathbb{R}$, dual of a[3] and define the following dual problem

$$\text{Find } \mathbf{u}^*\in\mathcal{V} \mid \forall\mathbf{v}\in\mathcal{V} \quad a^*(\mathbf{u}^*,\mathbf{v}) = J_T(\mathbf{v}) \tag{3.18}$$

[3] a^* is dual of a if and only if for all functions $\mathbf{u}$ and $\mathbf{v}$ in $\mathcal{V}$, $a^*(\mathbf{u},\mathbf{v}) = a(\mathbf{v},\mathbf{u})$. In the case where the differential operator present in a is self-adjoint, a is symmetric, and $a = a^*$.

Choosing $\mathbf{v} = \mathbf{e_u}$, the (unknown) error of the primal problem (3.6) in (3.18), the dual problem rewrites:

$$\begin{aligned} \text{Find } \mathbf{u}^* \in \mathcal{V} \mid a^*(\mathbf{u}^*, \mathbf{e_u}) &= J_T(\mathbf{e_u}) && (3.19)\\ a(\mathbf{e_u}, \mathbf{u}^*) &= J_T(\mathbf{e_u}) && (3.20) \end{aligned}$$

Define $\pi : \mathcal{V} \to \mathcal{V}_h$ a projector. As $\mathcal{V}_h \subset \mathcal{V}$, we can add/subtract any element of $\mathcal{V}_h$ to/from an element of $\mathcal{V}$, in particular $\pi\mathbf{u}^*$ to/from $\mathbf{u}^*$ and obtain

$$\begin{aligned} \text{Find } \mathbf{u}^* \in \mathcal{V} \mid \forall \pi\mathbf{u}^* \in \mathcal{V}_h \quad a(\mathbf{e_u}, \mathbf{u}^* + \pi\mathbf{u}^* - \pi\mathbf{u}^*) &= J_T(\mathbf{e_u}) && (3.21)\\ a(\mathbf{e_u}, \mathbf{u}^* - \pi\mathbf{u}^*) - \underbrace{a(\mathbf{e_u}, \underbrace{\pi\mathbf{u}^*}_{\in \mathcal{V}_h})}_{=0} &= J_T(\mathbf{e_u}) && (3.22) \end{aligned}$$

where the second term in (3.22) vanishes due to Galerkin orthogonality (Theorem 1.2.1. We are now left with the newly expressed dual problem

$$\text{Find } \mathbf{u}^* \in \mathcal{V} \mid \forall \pi\mathbf{u}^* \in \mathcal{V}_h \quad a(\mathbf{e_u}, \mathbf{u}^* - \pi\mathbf{u}^*) = J_T(\mathbf{e_u}) \tag{3.23}$$

The projector π is arbitrary, and we choose it so that $\pi\mathbf{u}^*$ is the finite element solution $\mathbf{u}_h^* \in \mathcal{V}_h$ to the discrete dual problem defined by[4]

$$\text{Find } \mathbf{u}_h^* \in \mathcal{V}_h \mid \forall \mathbf{v}_h \in \mathcal{V}_h \quad a^*(\mathbf{u}_h^*, \mathbf{v}_h) = J_T(\mathbf{v}_h), \tag{3.24}$$

and we obtain the final form of the dual problem we created

$$\begin{aligned} \text{Find } \mathbf{u}^* \in \mathcal{V} \mid a(\mathbf{e_u}, \mathbf{u}^* - \mathbf{u}_h^*) &= J_T(\mathbf{e_u}) && (3.25)\\ a(\mathbf{e_u}, \mathbf{e_{u^*}}) &= J_T(\mathbf{e_u}) && (3.26) \end{aligned}$$

This last form is a *representation* of the error on the J integral, but is still not computable since the exact errors $\mathbf{e_u}$ and $\mathbf{e_{u^*}}$ are in general not known. A *computable* error representation is easily obtained by replacing the exact primal solution $\mathbf{u}$ and its dual counterpart $\mathbf{u}^*$ by enhanced (recovered, smoothed) solutions $\widetilde{\mathbf{u}}$ and $\widetilde{\mathbf{u}^*}$. Defining the approximate errors $\mathbf{e}_{\widetilde{\mathbf{u}}} = \widetilde{\mathbf{u}} - \mathbf{u}_h$ and $\mathbf{e}_{\widetilde{\mathbf{u}^*}} = \widetilde{\mathbf{u}^*} - \mathbf{u}_h^*$ of the primal and dual problems, respectively, the expression for J_T in Equation (3.26) can then be approximated by

$$\text{Find } \mathbf{u}^* \in \mathcal{V} \mid a(\mathbf{e}_{\widetilde{\mathbf{u}}}, \mathbf{e}_{\widetilde{\mathbf{u}^*}}) \approx a(\mathbf{e_u}, \mathbf{e_{u^*}}) = J_T(\mathbf{e_u}) \tag{3.27}$$

Thus, all that remains is to compute the enhanced approximations $\widetilde{\mathbf{u}}$ and $\widetilde{\mathbf{u}^*}$. Note, however, that only gradients of the solutions appear in the bilinear form a. Enhanced solutions can for instance be computed by patch recovery techniques, or moving least square approximations.

IN SHORT:

The error on the functional of interest, here J writes $J(\mathbf{u}) - J(\mathbf{u}_h) = J_T(\mathbf{e_u})$ We now define the dual bilinear form $a^* : \mathcal{V} \times \mathcal{V} \to \mathbb{R}$ such that, for all $\mathbf{u}, \mathbf{v}$ in $\mathcal{V}$, we have $a^*(\mathbf{u}, \mathbf{v}) = a(\mathbf{v}, \mathbf{u})$. Let

[4] As for the primal problem, the discretized version (3.24) of the dual variational principle (3.23) yields a solution $\mathbf{u}_h^*$ which is not exact, and we note $\mathbf{e_{u^*}} = \mathbf{u}^* - \mathbf{u}_h^*$ the associated discretization error.

us define a dual problem as follows: find $\mathbf{u}^* \in \mathcal{V}$, such that, for all $\mathbf{v}$ in $\mathcal{V}$, $a^*(\mathbf{u}^*,\mathbf{v}) = J_T(\mathbf{v})$. We obtain $J_T(\mathbf{e_u}) = a^*(\mathbf{u}^*,\mathbf{e_u}) = a(\mathbf{e_{u^*}},\mathbf{e_u}) = a(\mathbf{u}^* - \mathbf{u}_h^*,\mathbf{e_u})$ For the linear elasticity problem, $a(\mathbf{e_{u^*}},\mathbf{e_u}) = \int_\Omega \left[\varepsilon(\mathbf{u}^*) - \varepsilon(\mathbf{u}_h^*)\right] : \mathbf{C} : [\varepsilon(\mathbf{u}) - \varepsilon(\mathbf{u}_h)]$

But, we know neither $\varepsilon(\mathbf{u})$ nor $\varepsilon(\mathbf{u}^*)$, hence, we use instead a good (smoothed, recovered, enhanced) solution for these two fields $\varepsilon(\mathbf{u}^*) \equiv \varepsilon(\mathbf{u}_h^*)$ and $\varepsilon(u) \equiv \varepsilon(uh)$

The error on the J integral functional is approximated by replaceing $\mathbf{u}_h$ by $\mathbf{u}_h$, the error on J writes $J(\mathbf{u}) - J(\mathbf{u}_h) \equiv J(\widetilde{u}_h) - J(\mathbf{u}_h)$.

Chapter 4

Measuring the error of extended finite element approximations

4.1 Need for error analysis of the XFEM

Recently, the finite element method (FEM) was extended. The extended finite element method (XFEM), based on an enrichment of the standard FEM permits a straightforward treatment of discontinuities and singularities where *neither meshing nor remeshing of the evolving discontinuity* is necessary. The main idea is to enrich the standard FE approximation locally with special functions that help capture some known feature of the solution such as discontinuities through cracks, material interfaces, near-crack-tip singularities, boundary layers... Only a few years since its academic inception [9], computational fracture mechanics software companies in fields such as aeronautics, geomechanics or the nuclear industry embraced the extended finite element method, which is now implemented in commercial packages.

As these course notes are written, engineers are deploying the XFEM to simulate crack propagation, assess damage tolerance and durability of structures in various engineering disciplines. As was the case of the FEM-engineers fifty years ago, today's XFEM-engineers are required to assess the accuracy of their calculations, and as the method gains popularity, this need will become all the more acute.

Despite the clear and stated need for validation and verification of numerical methods and the almost immediate uptake of XFEM research by industry, no work has been published on XFEM error estimation, save that of the PI and his collaborators. The Generalised Finite Element Method, close cousin to XFEM has been subject to more attention: [5, 6, 27], but much remains to be done in this context as well.

4.2 Need for error measures with specific goals

As previously stated, XFEM is employed industrially for fracture mechanics and reliability assessment, primarily in the context of linear elastic fracture mechanics (LEFM). The presence of initial defects (or cracks) is assumed, and their growth is governed by parameters known as *stress intensity factors*, which are sufficient to describe the state of stress in the vicinity of the crack fronts. From these, the fatigue life of a component may be determined by semi-empirical laws (e.g. Paris). Consequently, in LEFM, the critical quantities of interest are the stress intensity factors, which determine whether the material fails, the crack paths and the structure's fatigue life. The stress intensity factors are here the

quantity of interest and an adequate numerical method should minimise the error on this quantity of interest.

It is not evident that if the error in energy (EE) is minimised, then, the error on the stress intensity factors (SIFE) will also be minimal, even if experience shows that it will be reduced. The error distribution yielded by EE-minimisers will be quite different from that of an SIFE minimiser. Mathematics allow to eradicate this difficulty by providing *goal-oriented error estimates*. Such estimates date back to [15], and provide a means to minimise the error on a given quantity of interest (average stress in a region, displacement at a point, stress intensity factors...).

Through our on-going collaboration with leading experts in goal-oriented error estimation, (Korotov, Stein, Rüter), we propose to devise goal-oriented error estimators with the aim to tailor XFEM *approximation to the specific purposes of analysing cracks propagating in linear elastic media.*

The first steps in *goal-oriented error estimates for linear elastic fracture mechanics in a FE context* were taken by Rüter and Stein [24], and recent work by Dr Bordas, in collaboration with Dr Duflot, from the CENAERO started extending these techniques to the XFEM [12]. This work is based on the solution of a dual problem with the same left hand side, while the right hand side is computed based on the *goal* of the adaptive procedure.

4.3 Basic features of the error estimates

The rest of this chapter proposes and compares two *recovery based error estimation* techniques for *extended finite element methods, XFEM*, or, more generally, methods based on *extrinsic partition of unity enrichment*. The applications shown are in fracture mechanics, but the ideas are general and apply to any extrinsic enrichment scheme.

The first estimator employs derivative recovery with intrinsically enriched eXtended Moving Least Squares (XMLS) approximants and diffraction to account for the discontinuity through the crack. MLS derivative recovery in finite elements was first proposed in [28] of which this work is a generalization. The smoothness of the recovered derivatives is identical to that of the MLS weight function, in the examples proposed, they are C_1.

The second is a generalization to enriched approximations of the simple concept of *global derivative recovery* introduced in [17, 21] for the finite element method. The starting point of global derivative recovery is the remark that when only C_0 continuity of functions in the trial space is assumed in finite element methods, the strain and stress fields are discontinuous through element boundaries. The principle presented in [17, 21] is to construct an *enhanced* stress field interpolated with the same ansatzt functions as the displacements, and such that the L_2 norm *over the whole domain* of the difference between the enhanced and original finite element strains (stresses) is minimized. Through global minimization, we obtain an enhanced strain field, which is a better aproximant to the exact solution, itself unknown.

In both techniques, comparing the orginal (raw) XFEM strains to the enhanced strains, as in standard recovery-based error estimation [30], we define a local (element-wise) error which can be used to drive adaptive strategies.

The conclusions of the studies, reported in detail in [11], [10] [13] are that: (i) both XMLS and XGR methods yield error estimates which are valid, i.e. their effectivity tends to zero as the mesh is refined, (ii) the XMLS method yields smoother recovered fields than XGR, (iii) XGR is cheaper computationally than XMLS, at least in its initial formulation, (iv) XGR is more easily implemented in existing codes, and is well-suited to engineering analysis.

4.4 Essential results

For the sake of conciseness, we will only recall the key results associated with both estimators, and show how they are applied to three dimensional fracture problems. The readers are referred to [10, 11, 13] for details on the formulation and more numerical illustrations.

4.4.1 Extended moving least squares (XMLS) recovery

- The recovered strain/stress fields are C_1.
- In [10, 11], we show the necessity for the addition of the near-tip fields to the MLS basis, if these functions are not added, the effectivity index of the proposed error indicator does not tend to unity as the mesh is refined.
- For problems where the exact solution is not known, and thus where the effectivity index cannot be computed, we check that the L_2 norm of the difference between the raw XFEM strain field and the XMLS recovered strain field converges to zero with a rate close to the optimal rate of 1.0 as the mesh size tends to zero, as long as a fixed area is enriched around the crack tip during mesh refinement. If only the crack tip element is enriched, the convergence rate is close to $1/2$, which is the strength of the crack tip stress singularity. This corroborates the findings of References [7, 18]. Note that the higher the enrichment radius, the lower the error, the straighter the convergence line, and the closer to optimal the convergence rate is.
- Larger XMLS recovery smoothing lengths lead to higher effectivity indices, but we believe that the increase is not significant enough to justify the additional computational cost.
- In [10, 11], we show the superiority of the XMLS recovered solution with the now standard Superconvergent Patch Recovery (SPR) of [30], for fracture problems.

4.4.2 eXtended Global Recovery (XGR)

- The recovered strain/stress fields are C_0.
- The L_2 norm of the difference between the XGR strain and the raw XFEM strain vanishes upon mesh refinement.
- More importantly, we show that the effectivity index of the error indicator converges toward unity upon mesh refinement. This proves that the *approximate error* converges to the *exact error*, and, therefore, that the error indicator is indeed a correct measure of the error.
- The larger the XFEM enrichment radius, the closer the convergence rate is to 1. This corroborates earlier findings in the context of the XMLS recovery technique [10, 11] and is explained by the fact that larger enrichment radii lead to more accurate solutions, thus more accurate recovered solutions, and therefore an approximate error which is close to the exact error.
- Comparing the converged values of the effectivity index for XGR to that obtained for XMLS and published in [10, 11], we note that the XGR effectivities converge between 93 and 96%, whereas the XMLS effectivities are in the vicinity of 99%. For the whole range of mesh sizes, the XMLS effectivities are better than the XGR effectivities, this is due to the fact that the

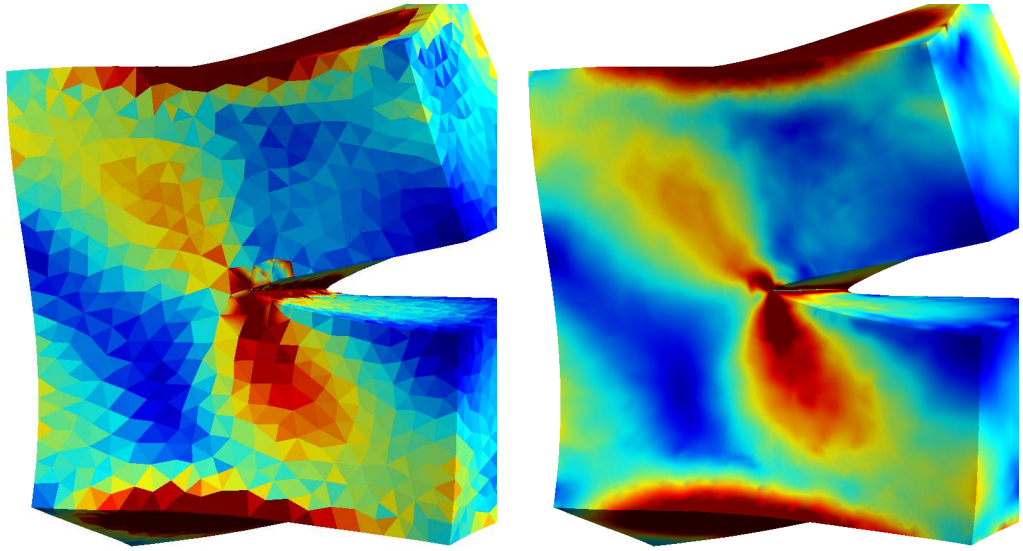

(a) Raw XFEM deformation field (b) Smoothed (recovered) deformation field

Figure 4.1: XMLS: deformed configuration and strain field for the combined tension/torsion loading case of the 3D crack. The smoothing fulfills its role nicely.

XMLS approximation is C_2 where as the XGR approximation is only C_0. We also notice that the XMLS results are less sensitive to the value of the enrichment radius than the XGR results. This is not surprising, since the XMLS recovery is built with a global intrinsic enrichment of the MLS approximation, whereas the enrichment used for the strain recovery in XGR is only active in a small[1] ball (tube) around the crack tip (front).

4.5 Three-dimensional illustrations

4.5.1 XMLS application

We show in this section the recovered derivatives for a 3D edge crack under combined tension and torsion loading. The domain is $[-1,1]\times[-1,1]\times[-0.5,0.5]$ ($x\times y\times z$). The crack is defined by the equation $y=0, x\leq 0$, its front is along the z axis. We show both the raw and enhanced strain field on the deformed configuration, so that the values on the faces of the crack, and along its front may be better identified. On face $y=1$, tractions are imposed as follows: $t_y=1$, $t_x=4z(1-x^2)$ and $t_z=4x(0.25-z^2)$. On face $y=-1$, tractions $t_y=-1$, $t_x=-4z(1-x^2)$ and $t_z=-4x(0.25-z^2)$ are imposed. Additionally, six nodal displacements are fixed so as to avoid rigid body modes. Figure 4.1 compares the deformation field obtained with the XFEM (a) to the recovered (smoothed) deformation field obtained through MLS derivative recovery. The results are quite satisfying.

4.5.2 XGR application

In this section, we summarize the three-dimensional example of a quarter-circular crack emanating from a hole in a cylindrical shell subjected to a uniform internal pressure. The elements are linear

[1] with respect to the domain size

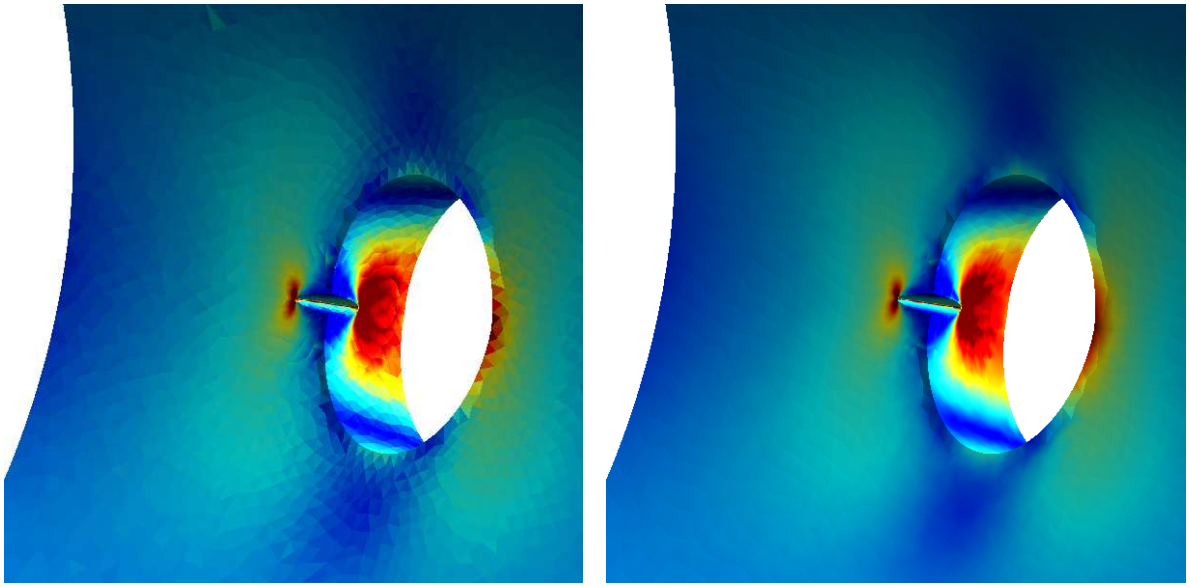

(a) raw XFEM strain field (b) XGR strain field

Figure 4.2: XGR: quarter-circular crack emanating from a hole in a cylindrical shell under internal pressure; the enrichment radius r_{enr} is equal to the radius of the quarter-penny crack.

tetrahedral elements. In this problem, elements in a tube centered on the crack front and with a variable radius r_{enr} are enriched with near-tip fields. The results are very interesting. They show that increasing the enrichment radius from $r_{crack}/5$ (roughly one element size) to r_{crack} decreases the error, and reduces the size of the *peak error zone*. For $r_{enr} = r_{crack}$, the estimated error around the crack front is approximately the same as the error on the other, uncracked side of the hole. This corroborates our findings in two dimensions, as well as the conclusions drawn in References [7, 18]. Results are shown in Figure 4.2.

4.6 Conclusions

We presented the basic results of our study of two a posteriori error estimates for the extended finite element method (XFEM). They suggest a strategy for $h-$adaptivity in enriched finite element methods, and hint at a new approximation adaptation scheme specifically taylored to enriched approximations. Indeed, it is clear that the error should be minimized by first *evaluating the optimal XFEM enrichment radius* r_{enr}[2] and, second, if the overall or/and local errors are still above the tolerance specified for the analysis at hand, proceed to $h-$ or/and $p-$ refinement, while keeping the enrichment radius constant. This procedure of estimating the optimal enrichment radius can be seen as a generalization of $h-$ and $p-$ adaptivity to encompass the non-polynomial functions present in the XFEM approximation. This new adaptivity could be coined *enrichment-adaptivity*, or *e-adaptivity*, and is subject to on-going research.

[2] this optimal enrichment radius is problem dependent. In our experience, it is situated in the vicinity of the length of the crack.

This page intentionally contains only this sentence.

Bibliography

[1] M. Ainsworth and J. T. Oden. A posteriori error estimation in finite element analysis. *Computer Methods in Applied Mechanics and Engineering*, 142:1–88, 1997.

[2] Mark Ainsworth and J. Tinsley Oden. *A posteriori error estimation in finite element analysis*. Wiley, 2000. ISBN: 0-471-29411-X.

[3] I. Babuška and W. C. Rheinboldt. Error estimates for adaptive finite element computations. *SIAM Journal of Numerical Analysis*, 15(4):736–754, August 1978.

[4] R. E. Bank and A. Weiser. Some a posteriori error estimators for elliptic partial differential equations. *Mathematics of computation*, 44:283–301, 1985.

[5] F. B. Barros, S. P. B. Proenca, and C. S. de Barcellos. Generalized finite element method in structural nonlinear analysis - a p adaptive strategy. *Computational Mechanics*, 33:95–107, 2004.

[6] F. B. Barros, S. P. B. Proenca, and C. S. de Barcellos. On error estimator and p-adaptivity in the generalized finite element method. *International Journal for Numerical Methods in Engineering*, 60:2373–2398, 2004.

[7] E. Béchet, H. Minnebo, N. Moës, and B. Burgardt. Improved implementation and robustness study of the x-fem for stress analysis around cracks. *International Journal for Numerical Methods in Engineering*, 2005.

[8] R. Becker and R. Rannacher. A feed-back approach to error control in finite element methods: Basic analysis and examples. *East-West J. Numer. Math.*, 4:237–264, 1996.

[9] T. Belytschko and T. Black. Elastic crack growth in finite elements with minimal remeshing. *International Journal for Numerical Methods in Engineering*, 45:601–620, 1999.

[10] S. Bordas and M. Duflot. Derivative recovery and a posteriori error estimation in extended finite element methods. *Computer Methods in Applied Mechanics and Engineering*, 2007. doi:10.1016/j.cma.2007.03.011.

[11] S. Bordas, M. Duflot, and P. Le. A simple a posteriori error estimator for the extended finite element method. *Communications in Numerical Methods in Engineering*, 2007. doi:10.1002/cnm.1001.

[12] S. Bordas, M. Rüter, M. Duflot, and S. Korotov. Goal-oriented a posteriori error estimates for the extended finite element method with applications to fracture mechanics. *Computer Methods in Applied Mechanics and Engineering*, submitted.

[13] M. Duflot and S. Bordas. An extended global recovery procedure for a posteriori error estimation in extended finite element methods. *International Journal for Numerical Methods in Engineering*, 2007. in press.

[14] K. Eriksson, D. Estep, P. Hansbo, and C. Johnson. Introduction to adaptive methods for differential equations. *Acta Numerica*, pages 106–158, 1995.

[15] K. Eriksson, D. Estep, P. Hansbo, and C Johnson. Introduction to adaptive methods for differential equations. *Acta Numerica*, pages 106–158, 1995.

[16] P. Heintz, F. Larsson, P. Hansbo, and K. Runesson. Adaptive strategies and error control for computing material forces in fracture mechanics. *International Journal for Numerical Methods in Engineering*, 60:1287–1299, 2004.

[17] E. Hinton and J.S. Campbell. Local and global smoothing of discontinuous finite element functions using a least squares method. *International Journal for Numerical Methods in Engineering*, 8, 1974.

[18] P. Laborde, J. Pommier, Y. Renard, and M. Salaun. High order extended finite element method for cracked domains. *International Journal for Numerical Methods in Engineering*, 190(47):6183—6200, 2004.

[19] P. Ladevèze and D. Leguillon. Error estimate procedure in the finite element method and applications. *SIAM Journal of Numerical Analysis*, 20:485–509, 1983.

[20] B. Moran and C.F. Shih. Crack tip and associated domain integrals from momentum and energy balance. *Engineering Fracture Mechanics*, 27:615–641, 1987.

[21] J.T. Oden and H.J. Brauchli. On the calculation of consistent stress distributions in finite element approximations. *International Journal for Numerical Methods in Engineering*, 3, 1971.

[22] L.F. Richardson. The approximate arithemtical solution by finite differences of physical problems. *Transactions of the Royal Society (London)*, 210:307–357, 1910.

[23] M. Rüter and E. Stein. Goal-oriented a posteriori error estimates in linear elastic fracture mechanics. *Computer Methods in Applied Mechanics and Engineering*, 195:251–278, 2006.

[24] Marcus Rüter and Erwin Stein. Goal-oriented a posteriori error estimates in linear elastic fracture mechanics. *Computer Methods in Applied Mechanics and Engineering*, 195:251–278, 2006.

[25] C.F. Shih, B. Moran, and T. Nakamura. Energy release rate along a three-dimensional crack front in a thermally stressed body. *Intern. J. of Fract.*, 30:79–102, 1986.

[26] P. Steinmann, D. Ackermann, and F.J. Barth. Application of material forces to hyperelastostatic fracture mechanics. ii. computational setting. 38:5509–5526, 2001.

[27] T. Strouboulis, L. Zhang, D. Wang, and I. Babuška. A posteriori error estimation for generalized finite element methods. *Computer Methods in Applied Mechanics and Engineering*, 195(9-12):852–879, February 2006.

[28] M. Tabbara, T. Blacker, and T. Belytschko. Finite element derivative recovery by moving least square interpolants. 117:211–223, 1994.

[29] Haijie Zhang, Stéphane Bordas, Marc Duflot, and Luxian Li. Residual-based error estimation for extended finite elements. *International Journal for Numerical Methods in Engineering*, 2007. submitted.

[30] O. C. Zienkiewicz and J. Z. Zhu. A simple error estimator and adaptive procedure for practical engineering analysis. *International Journal for Numerical Methods in Engineering*, 24:337–357, 1987.

[31] O. C. Zienkiewicz and J. Z. Zhu. The superconvergent patch recovery and a posteriori error estimates. Part 1: The recovery technique. *International Journal for Numerical Methods in Engineering*, 33:77:1331–1364, 1992.

[32] O. C. Zienkiewicz and J. Z. Zhu. The superconvergent patch recovery and a posteriori error estimates. Part 2: error estimates and adaptivity. *International Journal for Numerical Methods in Engineering*, 33:77:1365–1382, 1992.